J Mater Sci (2009) 44:700–707
DOI 10.1007/s10853-008-3188-7

Mechanical behavior of NiTi shape memory alloy fiber reinforced Sn matrix "smart" composites

J. P. Coughlin · J. J. Williams · N. Chawla

Received: 13 May 2008 / Accepted: 11 December 2008 / Published online: 13 January 2009

Abstract The detrimental effects of Pb on the environment and human health have provided the driving force for replacement of Pb–Sn solders with Pb-free alternatives. Sn-rich Pb-free solder alloys with silver and copper alloying additions have higher strength but lower elongation-to-failure than Pb–Sn solders. Thus, these alloys are more susceptible to failure under mechanical shock, drop, and thermal fatigue conditions. In this article, mechanical tensile testing of NiTi–Sn3.5Ag single fiber composites demonstrates superelastic behavior of the composite with 85% strain recovery. Fatigue experiments show an evolution in damage over cycles, and an S–N curve shows sharp transition between a nearly vertical low-cycle fatigue behavior and the high-cycle fatigue regime. The solder composite exhibits constant fatigue strength over the superelastic range of the NiTi fiber.

Introduction

Health concerns over Pb toxicity in traditional Pb–Sn solders have prompted the need for Pb-free solders in electronic packaging [1–3]. In general, Sn-rich solder alloys based on binary and ternary eutectics of Ag and Cu exhibit significant advantages in creep and thermal fatigue resistance over Pb–Sn solders [4–6]. These alloys also have inferior elongation-to-failure compared to Pb–Sn alloys. When these solder joints are subjected to mechanical stress during assembly, packaging, or in service, the poor elongation-to-failure may result in failure of the component [7, 8].

Shape memory alloys can be strained to levels as high as 4–6% with no significant permanent deformation. This is accomplished via two phase-transformation mechanisms: (a) Thermally induced transformation and (b) superelastic transformation. A superelastic transformation occurs when the shape memory alloy is strained in its austenite phase, above the austenite start temperature. After the sample is loaded above the strain required for transformation of the alloy, strain is recovered simply by unloading [9, 10].

The damage tolerance of Pb-free solder alloys may be improved by adding shape memory alloy (SMA) fibers to the Sn-rich solder matrix. Consider such a composite subjected to an externally applied stress along the direction of the fibers (Fig. 1). On loading, the fibers will undergo a superelastic transformation. When the applied stress is removed, the SMA fibers (as well as the solder matrix) should return to their original dimensions. Thus, embedding shape memory alloy fibers into a Pb-free solder alloy could potentially improve fatigue and mechanical shock properties of the material. NiTi alloys in particular have been studied extensively [11–19], and are a good choice as reinforcement in composites [20, 21] due to their relatively low-cost and non-toxicity. Binary 50–50 at.% NiTi alloys can have austenite finish temperatures, A_f, just below 0 °C, giving them a relatively wide superelastic range and making them excellent candidates for consumer electronics.

Preliminary study on NiTi-fiber/solder composites has been conducted by Dutta and co-workers [22–24]. They demonstrated that Pb-free solder/SMA composites show a decrease in permanent local displacement under an applied creep stress. The composite was heated and a shear stress was applied simultaneously, simulating strains induced by

J. P. Coughlin · J. J. Williams · N. Chawla (✉)
School of Materials, Fulton School of Engineering,
Arizona State University, Tempe, AZ 85287-8706, USA
e-mail: nchawla@asu.edu

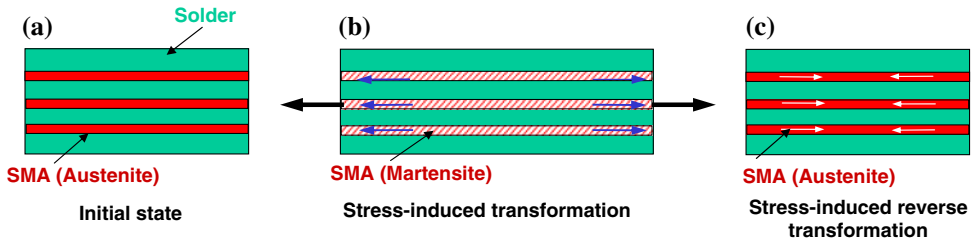

Fig. 1 **a** Shape memory alloy-reinforced Pb-free solder model system. **b** Upon application of an external force, load is transferred to the shape memory material, which undergoes superelastic transformation. **c** When the force is removed, a reverse transformation occurs, causing the composite to return to its original dimensions

CTE mismatch upon heading of an electronic package. They concluded that the observed recovery was due to thermal transformation of the NiTi reinforcement.

In this article, we examine the tension and fatigue behavior of a model single NiTi fiber-reinforced Sn–3.5Ag matrix composite. The damage-tolerant behavior of the composite is based on the superelastic behavior of the NiTi fiber. The efficiency of load transfer, and thus, transformation of the NiTi fiber is dependent on several factors including the aspect ratio of the reinforcement and the yield stress of the matrix. These important factors are considered and modeled analytically.

Materials and experimental procedure

NiTi fiber, (MPS118BB, 50 at.% Nickel, 50 at.% Titanium, Memry Corporation, Bethel, CT) was obtained after cold-drawing and guide-wire straightening to a diameter of 0.1 mm. The wire has also been annealed at 850 °C for 30 min followed by water quenching. Differential scanning calorimetry (DSC) was performed to determine the start and finish temperatures of both austenite and martensite.

The composite samples were fabricated by dip-coating the NiTi fiber in liquid Sn–3.5Ag alloy (Fig. 2). The wire was etched in an aqueous solution of 4.8% HF and 10.5% HNO_3 for 5 min to remove surface oxides. Sn–3.5Ag Pb-free solder was melted in a tapered ceramic crucible (30 mm in diameter) on a hot plate at a temperature of approximately 220 °C. The wire was dipped in a phosphoric acid-based flux (Indalloy flux #2, Indium Corporation, Utica, NY) and placed upright on a hot plate for 1 min to raise the temperature of the flux to approximately 100 °C (Fig. 2). When the Sn–Ag bath began to solidify, the wire was immersed and slowly removed, resulting in a uniform Sn–Ag matrix around a centered wire. The rate and temperature of this process was tailored to make composites with two volume fraction ranges: 2–5% and 6–10%. After dipping, the samples were air cooled.

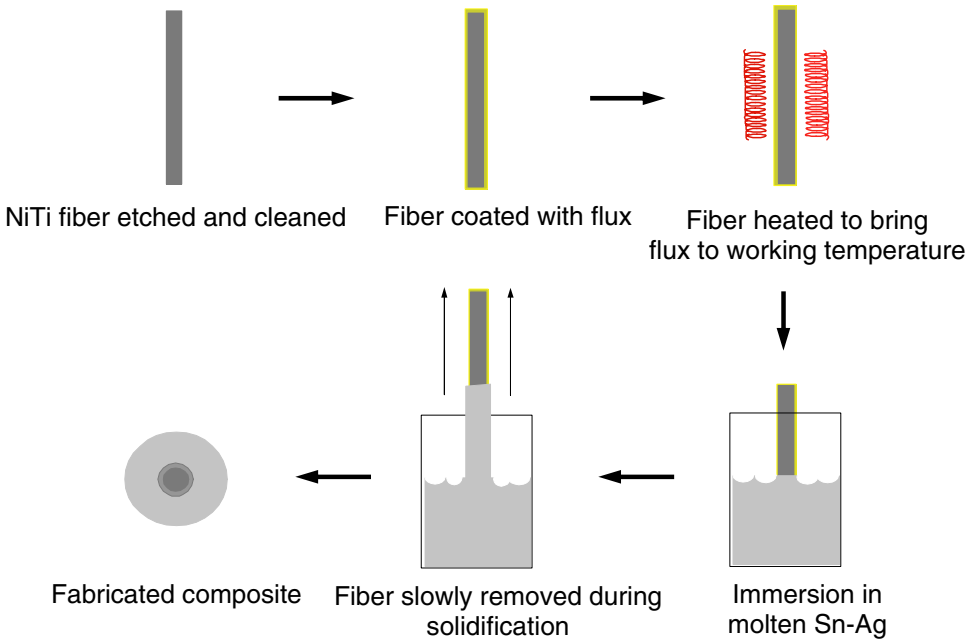

Fig. 2 Process used to fabricate bulk NiTi–Sn–Ag composites. Dip-coating at eutectic melting temperature (220 °C) provided good centering of the fiber and allowed control over volume fraction and sample quality

Composite preparation was completed by trimming each sample to a length, approximately, of 26 mm. Samples were then weighed and the final length and diameter were measured to estimate the volume fraction of fibers. Optical microscopy and image analysis were also used to verify the volume fraction measurements. Microstructural analysis was completed using a field emission gun scanning electron microscope (Hitachi S-4700, Tokyo, Japan). Backscattered electron imaging was used to obtain increased phase contrast and the energy dispersive spectroscopy (EDS) point analysis was used to determine phase composition.

Mechanical testing was performed on the single NiTi fiber, Sn–3.5Ag solder (Indium Corporation, Utica NY), and the composites using a microforce mechanical testing system (MTS Tytron 250, MTS Systems, Eden Prairie, MN) with a short-stroke displacement gauge and 250-N load cell. NiTi samples were clamped using flat grips and tested at various strain rates in strain control: 10^{-4}/s, 10^{-3}/s, and 10^{-2}/s. Because the strain was calculated using displacement and some compliance of the load train may be present, we do not report Young's modulus values. Unreinforced Sn–Ag samples were fabricated by drawing molten solder into Pyrex tubes (inner diameter of 2 mm) and allowing them to cool. Fatigue testing was performed in displacement control on NiTi–Sn–Ag composites at volume fractions ranging from 2% to 10% wire. At least 15 specimens were tested in fatigue. Each test was conducted at a frequency of 1 Hz (1 cycle per second), with an R-ratio ($\varepsilon_{min}/\varepsilon_{max}$) from 0.4 to 0.5 to prevent buckling of the sample. Fatigue run-out was defined as approximately 250,000 cycles.

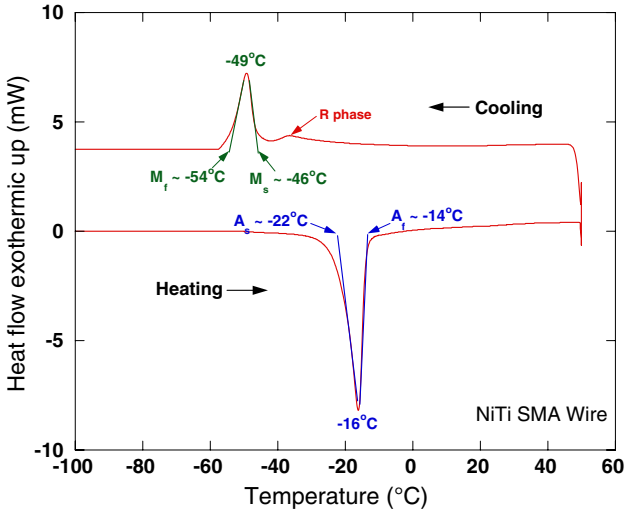

Fig. 3 Differential scanning calorimetry results show the NiTi shape memory alloy has transformation temperatures that are below freezing. This is beneficial to electronics applications because it allows superelastic transformation throughout the active (powered on) and inactive (powered off) temperature ranges where solder may be subject to damage

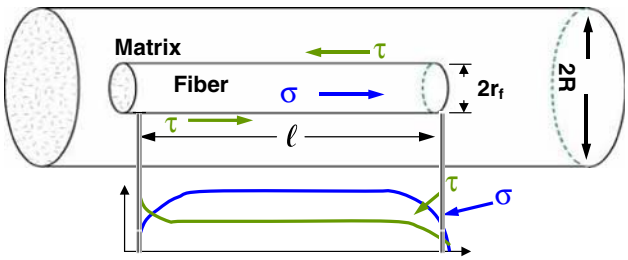

Fig. 4 Schematic illustrating tensile load transfer variables for a single fiber-reinforced system. In an SMA-reinforced Pb-free solder, the aspect ratio of the system must be large enough to reach the transformation stress in a superelastic reinforcement [9]

Results and discussion

The transformation temperatures of the NiTi fiber, obtained via DSC, are shown in Fig. 3. The transformation from martensite to austenite begins at −22 °C and ends at −14 °C, while the reverse transformation from austenite back to martensite occurs between −46 and −54 °C. These values correspond closely to those supplied by the manufacturer. The result is a superelastic temperature range between −14 and 250 °C, which is desirable for electronics applications because it allows superelastic transformation throughout the temperature ranges where solder is used.

In order to obtain the superelastic behavior in the composite, the aspect ratio of the fiber needs to be large enough for load transfer to take place, and create an average stress in the fiber equal or larger than the transformation stress. Figure 4 shows a schematic of load transfer in a fiber-reinforced composite. The critical aspect ratio needed to load the fiber to a stress σ_f, at the midpoint of the fiber, is given by the following equation [25]:

$$\left(\frac{l}{d}\right)_c = \left(\frac{\sigma_f}{2\tau_y}\right)$$

where l is length of the fiber, d is the diameter of the fiber (100 μm), σ_f is the stress in the fiber, and τ_y is the shear yield stress of the ductile matrix. Inspection of the previous equation shows that the average stress in the fiber will be significantly less than the transformation stress. Thus, in order to get significant transformation of the NiTi, the average stress in the wire needs to be well above the superelastic transformation stress of 450 MPa. In other words, the aspect ratio (l/d) needs to be much greater than the critical aspect ratio required to achieve this stress (Fig. 4). In order to achieve a stress greater than the transformation stress in the *majority* of the fibers, the following relation can be used [25]:

$$\bar{\sigma}_{\text{trans}} = \sigma_{\text{f}}\left(1 - \frac{1-\beta}{l/l_{\text{c}}}\right)$$

where l_{c} is the critical length for load transfer (from the previous equation) and l is the minimum length required to have an average stress ($\bar{\sigma}_{\text{trans}} = 450$ MPa). By definition, σ_{f} needs to be higher than $\bar{\sigma}_{\text{trans}}$, so we set it arbitrarily at 500 MPa (a value that is still lower than the ultimate tensile strength). β is a load transfer function, which for a perfectly plastic matrix is about 0.5. Using the above inputs, this translates to a minimum fiber length of 14 mm and a fiber aspect ratio of about 138. These dimensions were used to fabricate the single fiber composites.

Microstructural analysis of the NiTi–Sn–Ag composite shows a relatively well-centered fiber, well bonded to the matrix (Fig. 5). Perfect centering of the fiber was difficult because of the molten processing route employed. A very thin reaction zone consisting of a solid solution of primarily Sn and Ti with a small one out of Ni is formed, Fig. 5b. A detailed study of the interfacial reaction products and mechanisms is described elsewhere [26]. A comparison of the mechanical behavior of NiTi wire and bulk Sn–Ag solder is shown in Fig. 6. The SMA fiber exhibits full recovery after 3% strain, while the solder alloy exhibits a significant amount of permanent deformation. Figure 7 shows a comparison of the solder alloy with the single fiber NiTi solder matrix composite. The composite has a slightly higher yield stress than Sn–Ag solder, but demonstrates 85% strain recovery after unloading.

We now present the fatigue life results. There was no significant difference in fatigue behavior for the two groups of volume fractions (group 1—2–5 vol% and group 2—6–10 vol.%), so these are presented as one data set. Maximum strain versus cycles to failure (Fig. 8) and strain amplitude versus cycles to failure (Fig. 9) showed that samples fatigued above 0.4% strain failed between 1,500 and 5,500 cycles, regardless of maximum strain. Below 0.3–0.4% strain, the samples ran up to 250,000 cycles. This S–N curve behavior indicates that there is a sharp transition between low-cycle and high-cycle fatigue mechanisms. It is believed that low-cycle fatigue life is dominated by the superelastic transformation in the fiber. Because the fatigue tests were performed in strain control, the stress in the superelastic fiber between 1% and 3% strain does not vary

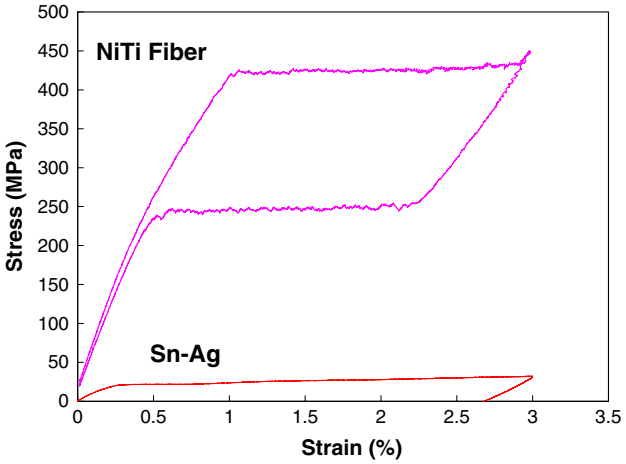

Fig. 6 Superelastic behavior of NiTi wire shows complete recovery of strain upon unloading, while Sn–3.5Ag solder does not show recovery of plastic strain

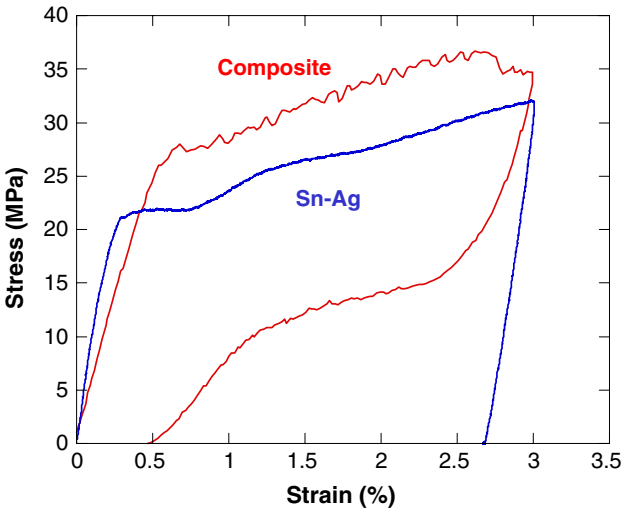

Fig. 7 Comparison of Sn–Ag and NiTi–Sn–Ag composite mechanical behavior at a strain rate of 10^{-4}/s shows recovery of 85% of the composite strain after unloading

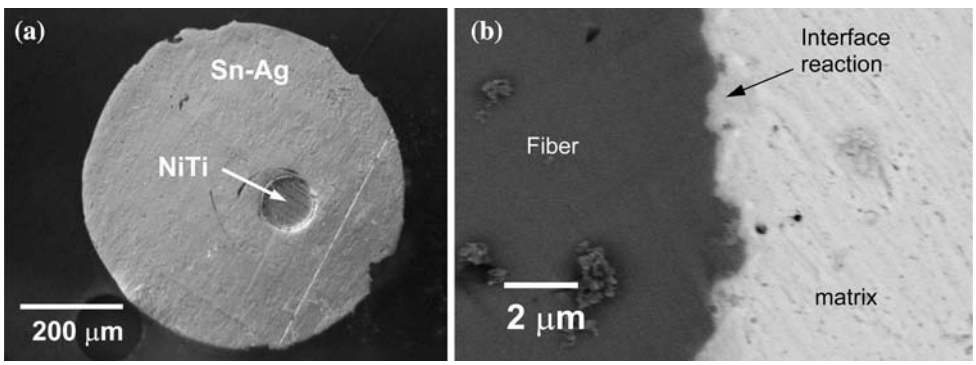

Fig. 5 **a** Cross-sectional analysis of NiTi–Sn3.5Ag solder sample shows good centering and wetting of the NiTi fiber. **b** Thin reaction layer at the fiber/matrix interface consisting of Sn–Ti–Ni solid solution

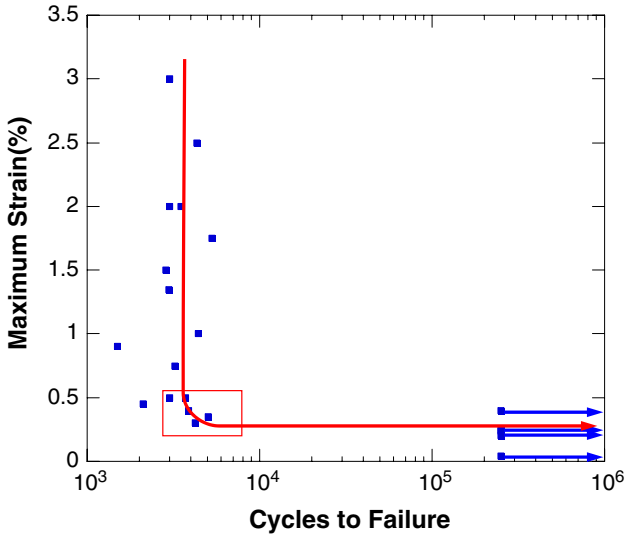

Fig. 8 Maximum strain versus number of cycles to failure for NiTi–Sn–Ag composites. Above 0.3% maximum strain, all the samples failed between 1,000 and 5,000 cycles regardless of volume fraction. Below 0.3% maximum strain, samples ran-out at 250,000 cycles

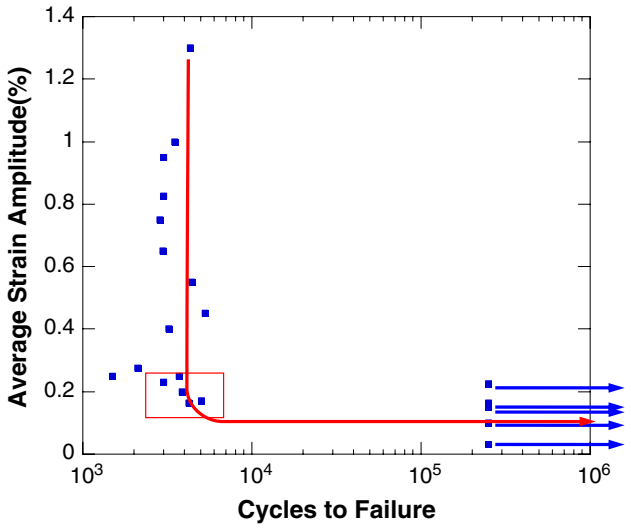

Fig. 9 Strain amplitude versus number of cycles to failure for NiTi–Sn3.5Ag composites. Above 0.3% maximum strain, all the samples failed between 1,000 and 5,000 cycles regardless of volume fraction. Below 0.3% maximum strain, samples ran-out at 250,000 cycles

significantly (because the stress–strain curve of the NiTi fiber is essentially horizontal over this strain range). Indeed, the fatigue life of the fiber over this narrow range seemed to be constant. Therefore, the fiber will exhibit the same fatigue life over this range. At lower strains, load transfer takes place but the stress on the fiber is not large enough to obtain transformation. The strains in the matrix are also very low, so the composite undergoes fatigue run-out. The transition from fatigue run-out to the "vertical" portion of the S–N curve can be directly correlated to the

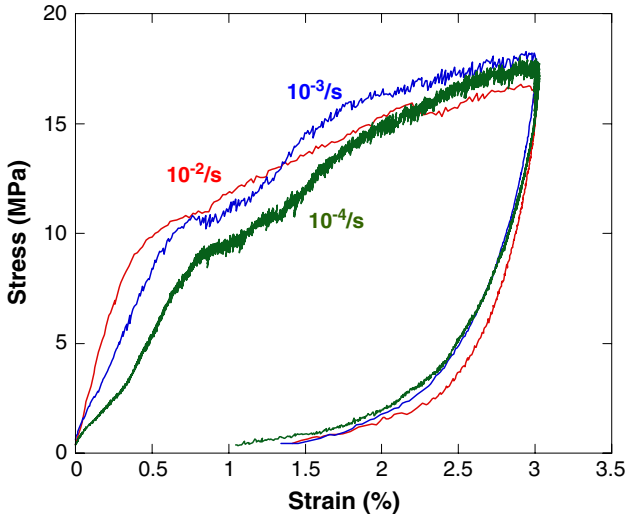

Fig. 10 Superelastic behavior of the composite at various strain rates ranging from 10^{-2}/s to 10^{-4}/s

onset of the proportional limit stress in the monotonic stress–strain curve of the fiber from Fig. 6.

Loading–unloading experiments were also conducted at various strain rates, ranging between 10^{-4}/s and 10^{-2}/s (Fig. 10), showing very little change in the hysteresis behavior. These experiments confirm that sufficient load transfer was present in the sample to reach transformation in the fiber at the given dimensions and loads, and that the entire composite demonstrated superelastic behavior.

The evolution of stress–strain hysteresis, at both high and low strains (Fig. 11) shows interesting behavior. Under high strain, clear superelastic transformation of the fiber is taking place. Plastic deformation accumulates in the matrix with increasing cycles, and fatigue damage is illustrated by a decreasing yield stress and narrower hysteresis. After 100 cycles, the matrix in the gauge section has accumulated a large amount of damage and no longer bears the majority of the load in the composite. Here, the hysteresis behavior closely resembles that of the NiTi fiber itself, suggesting that the fiber is the dominant load-bearing constituent. Finally, failure of the sample typically occurs between 3,000 and 5,000 cycles. For the low-strain sample, there is no evidence of transformation in the fiber because the stress in the fiber is not high enough. Because of the low strains, damage accumulation in the matrix is slower than for the high-strain samples. Therefore, these samples ran-out at 250,000 cycles.

The decrease of maximum stress over number of cycles in the composite is attributed to cyclic softening and damage in the matrix, caused by superelastic transformation of the fiber. This results in the NiTi fiber carrying the majority of the load. The higher strain samples show a more rapid decrease in maximum stress over time,

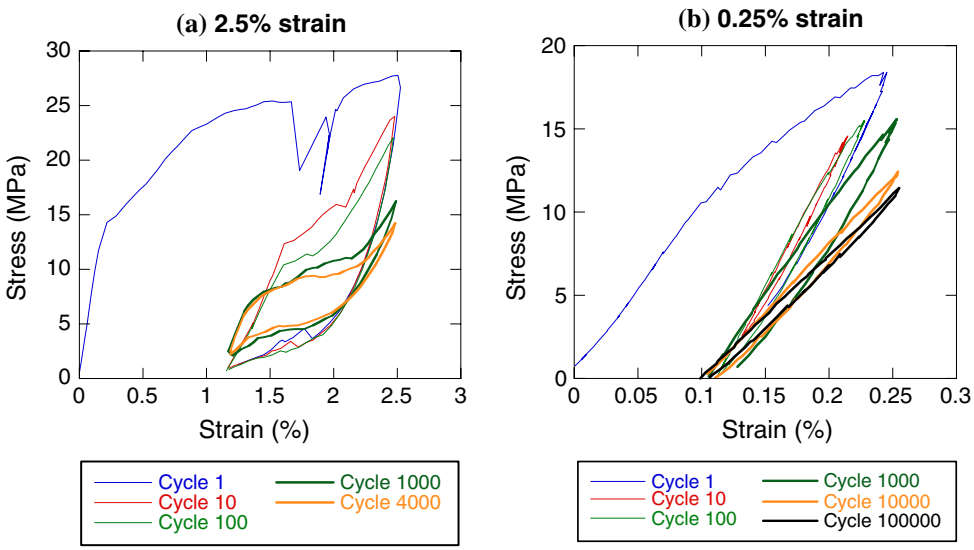

Fig. 11 Fatigue behavior of composite samples at **a** 2.5% strain and **b** 0.25% strain, showing evolution of hysteresis behavior as damage increases in the Sn–Ag matrix. The superelastic transformation is visible at strains above 0.4%, and those samples typically fractured between 2,000 and 5,000 cycles, while samples at very low strains did not show a transformation, and did not fracture

followed by failure. The lower strain samples do not have as steep as of a slope and ran-out at 250,000 cycles.

A schematic illustrating the possible sequence in damage evolution is shown in Fig. 12. The fiber undergoes superelastic transformation, while the matrix undergoes plastic deformation. Any residual stress is likely relieved by plastic deformation of the matrix in the first cycle. Unloading allows the fiber to return to its original dimensions, but causes reverse plastic deformation in the matrix.

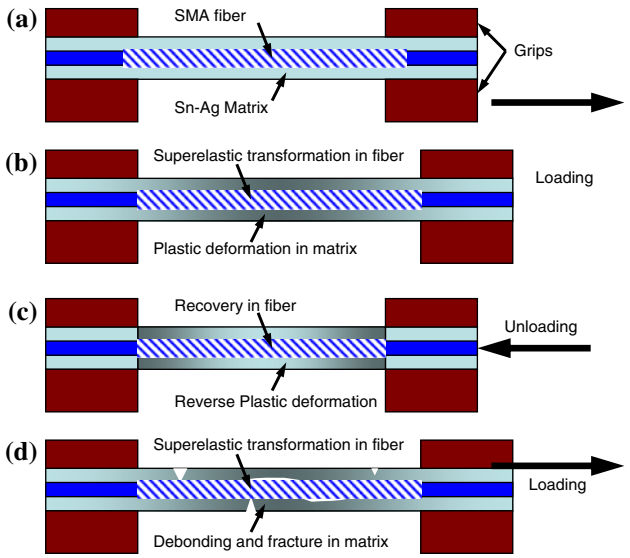

Fig. 12 Damage evolution in NiTi/Sn–Ag composite due to fatigue. **a** The sample was loaded in tension. **b** The wire undergoes superelastic transformation, while the matrix undergoes plastic deformation. **c** Unloading allows the fiber to return to its original dimensions, but causes reverse plastic deformation in the matrix. **d** Subsequent loading and unloading cause more plastic deformation and hardening of the matrix, resulting in decohesion on the fiber/matrix interface and fracture of the matrix itself. The NiTi wire bears more of the load over an increasing number of cycles

Subsequent loading and unloading cause more plastic deformation of the matrix, resulting in decohesion on the fiber/matrix interface and fracture of the matrix itself. The NiTi fiber bears more of the load over an increasing number of cycles. Fractography performed on the fatigue samples (Fig. 13) showed necking of the matrix, indicating plastic deformation. Debonding of the matrix from the fiber can be seen because of damage accumulated near the interface during cycling. Some residual matrix shown attached to the fiber (Fig. 14) indicates that debonding actually occurs within the matrix, indicating that the fiber/matrix bond strength was relatively good. Fractography of the wire shows brittle fracture where the crack originated and ductile fracture at the opposite side of the fiber, indicating rapid fracture and suggesting that the fiber was bearing the majority of the load at failure.

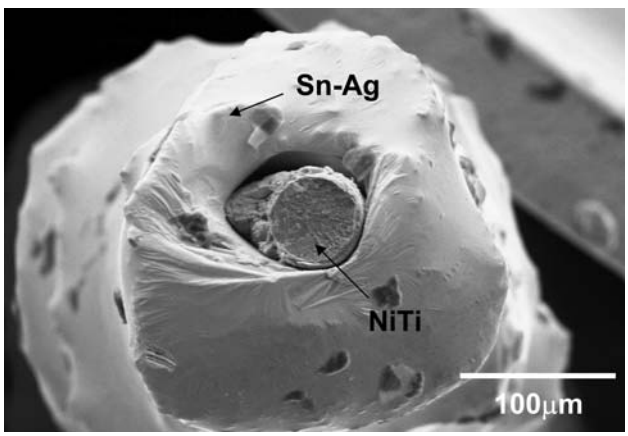

Fig. 13 Fractography of single fiber composite after fatigue failure. Smooth striations in matrix and necking of the composite indicate plastic deformation. Debonding is present at NiTi/Sn–Ag interface, with residual Sn–Ag still adhered to the fiber

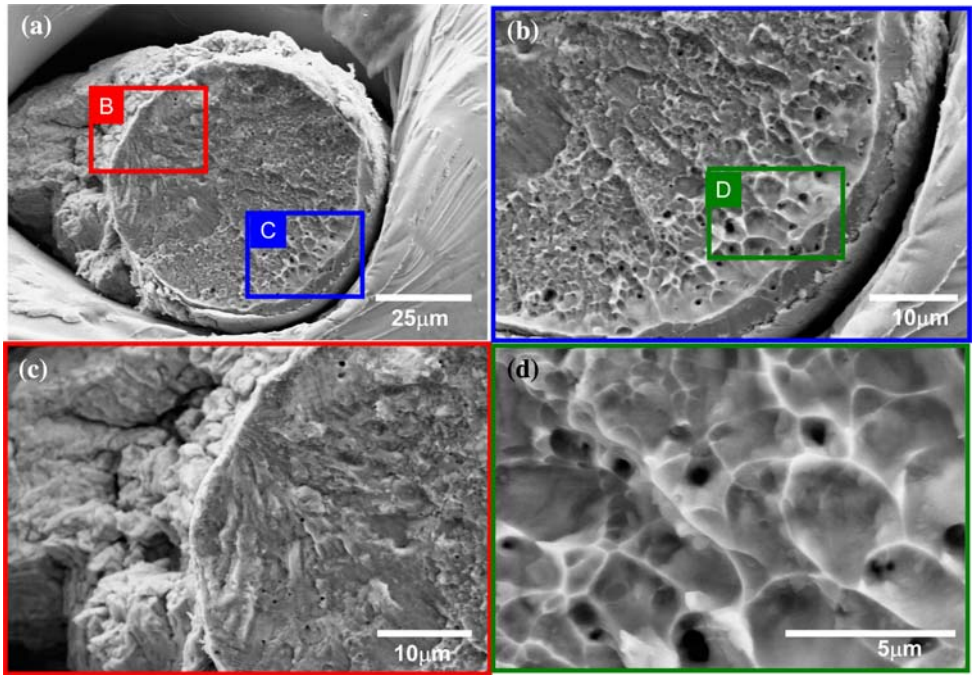

Fig. 14 SEM of NiTi–Sn–Ag fatigue specimen at fracture surface. **a** Debonding occurs between fiber and matrix due to damage accumulation at the interface, with residual Sn–3.5Ag matrix remaining bonded to the fiber surface. Fracture of the fiber results in two types of fractures, **b** brittle and (**c**, **d**) ductile

Summary

Mechanical testing of a superelastic NiTi single fiber-reinforced Sn–3.5Ag matrix composite was performed to investigate the effect of superelastic transformation on the mechanical properties of Pb-free solders. The following conclusions can be made:

- Differential scanning calorimetry of the NiTi fiber revealed the start and finish temperatures of both austenite and martensite.
- A critical aspect ratio of 138 was calculated for significant load transfer to induce superelastic transformation over the length of the fiber. A recovery of 85% of the permanent strain was observed during initial cycling at strain rates varying between 10^{-4} and 10^{-2}.
- Fatigue testing showed failure between 3,000 and 5,000 cycles above 0.3% maximum strain, and run-outs occurred at 250,000 cycles below 0.3% maximum strain. Damage to the Sn–Ag matrix during run-outs occurred mainly within the first 100 cycles. Fatigue life was controlled by the fiber, which was bearing the majority of load at failure.
- The nature of the strain-controlled fatigue test coupled with the superelastic behavior in the fiber resulted in a very steep fatigue curve with a sharp transition between low-cycle and high-cycle fatigue. The "anomalous" fatigue behavior can be attributed to the superelastic nature of the fiber, which results in a constant stress over a range of applied strain.
- Fractographic analysis showed a good bond between fiber and matrix, as exemplified by a thin layer of matrix adhering to the fiber after fracture.

Acknowledgements The authors acknowledge financial support for this research from Intel Corporation (Dr. D. Suh, Dr. R. Mahajan, and Dr. V. Wakharkar). The authors also thank Gordon Moore from the Department of Chemistry and Biochemistry at Arizona State University for his help with the WDS, and the Memry Corporation for providing the NiTi fibers used in this study.

References

1. Kang S, Sarkhel AK (1994) J Electron Mater 23:701
2. Frear DR, Vianco PT (1994) Metall Trans A 25:1509
3. Glazer J (1995) Int Mater Rev 40:65
4. Abtew M, Selvaduray G (2000) Mater Sci Eng R Rep 27:95
5. Plumridge WJ (2005) Monatsh Chem 136:1811
6. Vianco PT, Frear DR (1993) J Electron Mater 45:14
7. Choi S, Subramanian KN, Lucas JP, Bieler TR (2000) J Electron Mater 29:1249
8. Terashima S, Yoshiharu K, Takuya H, Masamoto T (2003) J Electron Mater 32:1527
9. Chawla N, Chawla KK (2006) Metal matrix composites. Springer Press, New York
10. Otsuka K, Wayman CM (1998) Shape memory materials. Cambridge University Press, Cambridge, United Kingdom
11. Frick CP, Ortega AM, Tyber J, Maksound A, Maier HJ, Liu Y, Gall K (2005) Mater Sci Eng A 405:34
12. Shimamoto A, Zhao HY, Abe H (2004) Int J Fatigue 26:533
13. Vokoun D, Kafka V, Hu CT (2003) Smart Mater Struct 12:680
14. Wagner M, Sawaguchi T, Kausträter G, Höffken D, Eggeler G (2004) Mater Sci Eng A 378:105
15. Wang ZG, Zua XT, Fub YQ, Wang LM (2005) Thermochim Acta 428:199

16. Young JM, Van Vliet KJ (2005) J Biomed Mater Res 72:17
17. Zheng Y, Cui L, Schrooten J (2004) Appl Phys Lett 84:31
18. Brinson LC, Schmidtb I, Lammering R (2004) J Mech Phys Solids 52:1549
19. Liu JY, Lu H, Chen JM, Alain C, Wu T (2008) J Mater Sci 43:4921. doi:10.1007/s10853-008-2716-9
20. Wei ZG, Sandstrom R, Miyazaki S (1998) J Mater Sci 33:3763. doi:10.1023/A:1004674630156
21. Boccaccini AR, Peters C, Roether JA, Eifler D, Misra SK, Minay EJ (2006) J Mater Sci 41:8152. doi:10.1007/s10853-006-0556-z
22. Dutta I, Majumdar BS, Pan D, Horton WS, Wright W, Wang ZX (2004) J Electron Mater 33:258
23. Wang ZX, Dutta I, Majumdar BS (2006) Scripta Mater 54:627
24. Wang ZX, Dutta I, Majumdar BS (2006) Mater Sci Eng A 421:133
25. Kelly A (1987) Strong solids. Clarendon Press, Oxford, p 157
26. Coughlin JP, Williams JJ, Crawford GA, Chawla N (2009) Metall Mater Trans A (in press)